Molecules and Cells

A Novel Tetrameric Assembly Configuration in VV2_1132, a LysR-Type Transcriptional Regulator in *Vibrio vulnificus*

Yongdae Jang[1], Garam Choi[1,2], Seokho Hong[1], Inseong Jo[1], Jinsook Ahn[1], Sang Ho Choi[1,2,*], and Nam-Chul Ha[1,*]

[1]Research Institute for Agriculture and Life Sciences, Center for Food and Bioconvergence, Center for Food Safety and Toxicology, Seoul National University, Seoul 08826, Korea, [2]National Research Laboratory of Molecular Microbiology and Toxicology, Seoul National University, Seoul 08826, Korea
*Correspondence: choish@snu.ac.kr (SHC); hanc210@snu.ac.kr (NCH)
http://dx.doi.org/10.14348/molcells.2018.2190
www.molcells.org

LysR-type transcriptional regulators (LTTRs) contain an N-terminal DNA binding domain (DBD) and a C-terminal regulatory domain (RD). Typically, LTTRs function as homotetramers. VV2_1132 was identified in *Vibrio vulnificus* as an LTTR that is a homologue of HypT (also known as YjiE or QseD) in *Escherichia coli*. In this study, we determined the crystal structure of full-length VV2_1132 at a resolution of 2.2 Å, thereby revealing a novel combination of the domains in the tetrameric assembly. Only one DBD dimer in the tetramer can bind to DNA, because the DNA binding motifs of the other DBD dimer are completely buried in the tetrameric assembly. Structural and functional analyses of VV2_1132 suggest that it might not perform the same role as *E. coli* HypT, indicating that further study is required to elucidate the function of this gene in *V. vulnificus*. The unique structure of VV2_1132 extends our knowledge of LTTR function and mechanisms of action.

Keywords: LysR type transcriptional regulator, *Vibrio vulnificus*, X-ray crystallography

INTRODUCTION

LysR-type transcriptional regulators (LTTRs) comprise the largest family of transcriptional regulators in prokaryotes and play diverse biological roles in virulence, motility, quorum sensing, and scavenging of oxidative stressors (Maddocks and Oyston, 2008). For instance, OxyR induces the transcription of many proteins scavenging the oxidative stresses by sensing the low level of H_2O_2 (Jo et al., 2017; Maddocks and Oyston, 2008). LTTRs share a common structural architecture consisting of an N-terminal DNA binding domain (DBD) and a C-terminal regulatory domain (RD), which are connected by a long linker helix in the DBD (Maddocks and Oyston, 2008; Muraoka et al., 2003). Crystal structures of LTTRs have revealed that the RD adopts two Rossmann fold-like subdomains (RD-I and RD-II) to recognize cognate ligands or stimuli (Choi et al., 2001; Lochowska et al., 2001; Park et al., 2017a). The DBD forms a stable dimer that thus has a pair of winged helix-turn-helix (wHTH) motifs for palindromic DNA binding (Alanazi et al., 2013; Choi et al., 2001; Jo et al., 2015; Maddocks and Oyston, 2008). The DBD contains a long linker helix with a hinge region that connects to the RD and consists of a flexible stretch of amino acids, providing interdomain flexibility.

Most LTTRs adopt a homotetrameric assembly in an asymmetric two dimer arrangement, since each dimer is composed of two subunits in different conformations between the DBD and the RD (Muraoka et al., 2003). In the

Received 4 September, 2017; revised 3 November, 2017; accepted 8 January, 2018; published online 27 February, 2018

eISSN: 0219-1032

tetramer, both DBD dimers are located at the bottom of the main body, which consists of two RD dimers facing each other. This arrangement of DBD dimers in the tetramer appears suited for binding to a DNA sequence composed of two (pseudo)palindromic sequences (Jo et al., 2015). The distance between the two DBD dimers is affected by ligand binding to the RDs, which controls DNA binding (Jo et al., 2015; Maddocks and Oyston, 2008).

Escherichia coli has many LTTRs in its genome. LTTR QseD (also known as YjiE) was initially identified as a regulator of quorum sensing and cell motility (Habdas et al., 2010). Deletion of *qseD* in *Escherichia coli* K-12 yielded a mutant strain with a phenotype of increased motility that is associated with quorum sensing (Habdas et al., 2010). Later, QseE was also termed HypT (hypochlorite-responsive transcription factor) because this gene is a transcriptional regulator involved in hypochlorite resistance in *E. coli* (Drazic et al., 2014; Gebendorfer et al., 2012). Oxidation of three methionine residues and one cysteine residue was proposed to be a key step for sensing HOCl in *E. coli* HypT (Drazic et al., 2013a; Drazic et al., 2013b). However, the molecular mechanism of this sensing and the oligomerization state of the protein remain to be elucidated.

Vibrio vulnificus is a highly pathogenic Gram-negative bacterium that can cause fatal septicemia, especially in immunocompromised individuals (Jones and Oliver, 2009). The VV2_1132 gene (accession number AAO08033.2) was identified in the *V. vulnificus* CMCP6 genome (accession number GCA_000039765.1) (Kim et al., 2011b) as an orthologue of *E. coli* HypT. Sequence alignment revealed that VV2_1132 shows 30% and 29% sequence identity to *E. coli* HypT and its homologue in *Salmonella enterica* serovar Typhimurium (accession number WP_000383509), respectively (Jang et al., 2017). Here, we determine the crystal structure of the full-length VV2_1132 protein, thereby revealing a novel configuration in its tetramer formation. We also discuss possible ligand binding sites and potential mechanisms by which this protein is regulated.

MATERIALS AND METHODS

DNA constructs, protein expression, and purification

The DNA constructs, protein expression, and purification of VV2_1132 have been previously described (Jang et al., 2017). Briefly, the gene for VV2_1132 was cloned into the pProEx-HTa vector (Invitrogen, USA), resulting in pProEX-HTa-VV2_1132. The VV2_1132 protein was overexpressed in *E. coli* BL21 (DE3) cells harboring pProEX-HTa-VV2_1132 and purified using three different chromatographic columns: Ni-NTA affinity, Q anion-exchange, and size exclusion chromatography. The final protein was concentrated to 9 mg/mL in a buffer containing 20 mM Tris (pH 8.0), 150 mM NaBr, and 2 mM β-mercaptoethanol and then stored at -80℃ until use.

For production of SeMet-labeled protein, B834 (DE3) cells were transformed with the recombinant pProEx-HTa VV2_1132 plasmid. Cells were cultured in M9 medium supplemented with an amino acid mixture containing L-(+)-selenomethionine, 100 μg/mL ampicillin, and other cofactors (Guerrero et al., 2001). Cells were harvested, disrupted, and purified by the same method as for the native VV2_1132. The protein was concentrated to 9 mg/mL; stored in a buffer containing 20 mM Tris (pH 8.0), 150 mM NaCl, and 2 mM β-mercaptoethanol; and frozen at -80℃ until use.

Size-exclusion chromatography with multi-angle light scattering (SEC-MALS)

SEC-MALS experiments were performed using a High-performance liquid chromatography pump (Agilent) connected to a Superdex-200 10/300 GL (GE Healthcare) gel filtration column and a Wyatt DAWN HELIOS MALS instrument. The gel filtration column was pre-equilibrated with 20 mM Tris-HCl (pH 7.5), 150 mM NaCl, 2 mM β-mercaptoethanol. Bovine serum albumin at 2 mg/mL was used as a protein standard. The VV2_1132 protein sample at 3 mg/mL was injected into the column and eluted at a flow rate of 0.2 ml/min. The data were evaluated using the debye model for static light scattering data fitting and represented using an EASI graph with a RI peak in the ASTRA V software (Wyatt).

Crystallization, data collection, and structural determination of SeMet-labeled VV2_1132

Native VV2_1132 protein was crystallized in precipitation solution containing 0.1 M imidazole (pH 7.6), 0.9 M ammonium phosphate dibasic, 0.2 M NaBr, and 2 mM TCEP at 14℃, as reported previously (Jang et al., 2017). SeMet-labeled VV2_1132 protein was crystallized under a precipitation solution containing 0.1 M imidazole (pH 7.6), 0.9 M ammonium phosphate dibasic, 0.2 M NaCl, and 2 mM TCEP. To collect the X-ray diffraction dataset, native and SeMet-labeled crystals were transferred for 1 min to 2 μl of cryoprotection buffer containing the precipitation solution supplemented with 30% sorbitol, after which the crystals were flash-cooled in liquid nitrogen. The diffraction dataset was collected using an undulator X-ray beam (beamline 5C in the Pohang Accelerator Laboratory, Pohang, Republic of Korea) (Park et al., 2017b) at a wavelength of 0.9801 Å. The native crystal belonged to the space group of $P2_12_12$ with unit cell parameters a = 57.8, b = 113.5, and c = 220.7 Å. The SeMet-labeled crystal belonged to the space group of $P2_12_12$ with unit cell parameters a = 114.3, b = 115.9, and c = 221.9 Å. Complete diffraction datasets of the native crystals were subsequently processed, merged, and scaled with HKL-2000 to a resolution of 2.2 Å. Datasets of the SeMet-labeled crystals were diffracted up to a resolution of 2.4 Å (Otwinowski and Minor, 1997). Data collection statistics are provided in Table 1. Anomalous signals from four Se sites were found in each subunit, and the resulting electron density map was sufficiently clear to build an initial model using the programs PHENIX and COOT (Adams et al., 2010; Emsley and Cowtan, 2004). To solve the crystal structure of the native VV2_1132 protein at 2.2 Å resolution, molecular replacement was carried out against the native diffraction dataset using the initial model as a search model in the program MOLREP in the CCP4 suite (Winn et al., 2011).

Table 1. X-ray diffraction and refinement statistics

	SeMet VV2_1132	Native VV2_1132
Data collection		
Beam line	PAL 5C	PAL 5C
Wavelength (Å)	0.98010	1.00820
Space group	$P2_12_12$	$P2_12_12$
Cell dimensions		
a, b, c (Å)	57.5, 111.1, 219.30	57.8, 113.5, 220.7
α, β, γ (°)	90, 90, 90	90, 90, 90
Resolution (Å)	50.0-3.00 (3.05-3.00)	50.0-2.20 (2.24-2.20)
R_{merge}	0.104 (0.346)	0.061 (0.494)
R_{pim}	0.033 (0.133)	0.019 (0.214)
High resolution shell CC1/2	0.740	0.219
$I/\sigma I$	16.6 (3.4)	56.4 (4.5)
Completeness (%)	98.8 (98.0)	93.7(83,8)
Redundancy	8.3 (5.8)	8.3 (4.6)
Refinement		
Resolution (Å)		2.20
No. of reflections		65417
R_{work}/R_{free}		0.2017/0.2636
No. of total atoms		9223
Wilson B-factor (Å)		2471
R.M.S. deviations		
Bond lengths (Å)		0.008
Bond angles (°)		0.955
Ramachandran plot		
Favored (%)		95.39
Allowed (%)		4.43
Outliers (%)		0.18
PDB ID		5Y9S

* Values in parentheses are for the highest resolution shell.

Strains, plasmids, and culture conditions

The strains and plasmids used in this study are listed in Table 2. Unless otherwise noted, *V. vulnificus* strains were grown at 30℃ in LB medium supplemented with 2% (*wt/vol*) NaCl (LBS).

Construction of the VV2_1132 mutant strain

The VV2_1132 gene was inactivated *in vitro* by deletion of the VV2_1132 open reading frame (ORF) using a PCR-mediated linker-scanning mutation method as described previously (Jang et al., 2016). Primers VV21132_F1_F and _R (for amplification of the 5′-amplicon) and VV21132_F2_F and _R (for amplification of the 3′-amplicon) were used as listed in Table 3. The 566-bp deleted VV2_1132 region was amplified by PCR using a mixture of both amplicons as the template and VV21132_F1_F and VV21132_F2_R as primers. The resulting ΔVV2_1132 amplicon was ligated with Spe I -Sph I -digested pDM4 (Milton et al., 1996) to generate pGR1618 (Table 2). The *E. coli* S17-1λ*pir*, *tra* strain (Simon et al., 1983), which contains pGR1618, was used as a conjugal donor to *V. vulnificus* CMCP6 (Table 2). Conjugation and isolation of the transconjugants were conducted as described previously (Kim et al., 2011a). The resulting *V. vulnificus* VV2_1132 mutant was named GR1619 (Table 2).

Growth kinetics under HOCl stress

Wild-type *V. vulnificus* and the VV2_1132 mutant were grown in M9 minimal medium supplemented with 0.4% (*wt/vol*) glucose (Sambrook et al., 2006), after which they were exposed to 3.81, 6.67, or 9.53 μM of NaOCl (Sigma-Aldrich, USA). Cell growth was monitored spectrophotometrically at 600 nm (OD_{600}) with a microplate reader (Tecan Infinite M200 reader, Switzerland).

Motility test

Bacterial motility was tested as described previously (Lim and Choi, 2014). Wild-type *V. vulnificus* and the VV2_1132 mutant were grown to an OD_{600} of 0.5 and subsequently stabbed into LBS semisolid medium solidified with 0.3% (*wt/vol*) agar. The plates were incubated at 30℃ for 18 h, after which migration through the agar was photographed using a Gel Doc™ EZ imager (Bio-Rad, USA).

Table 2. Plasmids and bacterial strains used in this study

Strain or plasmid	Relevant characteristics[a]	Reference or source
Bacterial strains		
V. vulnificus		
CMCP6	Clinical isolate; virulent	Laboratory collection
GR1619	CMCP6 with ΔVV2_1132	This study
E. coli		
S17-1λ*pir*	λ-*pir* lysogen; *thi pro hsdR hsdM*$^{+}$ *recA* RP4-2 Tc::Mu-Km::Tn7;Tp^{r} Sm^{r}; host for π-requiring plasmids; conjugal donor	Simon *et al.*, 1983
BL21(DE3)	*F* ompT hsdS (rB^{-}mB^{-}) gal (DE3)	Laboratory collection
Plasmids		
pProEx-HTa	His6-tag fusion protein expression vector; Ap^{r}	Invitrogen
pDM4	R6K γ *ori sacB*; suicide vector; *oriT* of RP4; Cm^{r}	Milton *et al.*, 1996
pGR1618	pDM4 with ΔVV2_1132; Cm^{r}	This study

[a] Tp^{r}, trimethoprim resistant; Sm^{r}, streptomycin resistant; Cm^{r}, chloramphenicol resistant.

Table 3. Oligonucleotides used in this study

Name	Oligonucleotide Sequence (5′ → 3′)[a, b]	Use
For mutant construction		
VV21132_F1_F	GTATTTCCTTGCTCTGCCCATCC	Deletion of VV2_1132 ORF
VV21132_F1_R	ACTGGATCCGATTGCGTAACAAAG	
VV21132_F2_F	ATCGGATCCAGTCTTTGAAACCAC	Deletion of VV2_1132 ORF
VV21132_F2_R	GGCCTTTTTTATTAAGTAGTTGGTCAGATC	
For expression construction		
VV21132_Ex_F	GGTCCATGGCTATGAATAACCCACTAGAATTC	Overexpression of VV2_1132
VV21132_Ex_R	GGTCTCGAGTTATGACTTGTCGATTTCTTGCC	

[a] Oligonucleotides were designed using the *V. vulnificus* CMCP6 genomic sequence (GenBank™ accession number CE016795 and CE016796, www.ncbi.nlm.nih.gov).
[b] Regions of oligonucleotides not complementary to the corresponding gene are underlined.

RESULTS

Structural determination and overall structure of VV2_1132

Full-length VV2_1132 protein was successfully produced in the *E. coli* expression system and purified to homogeneity, as described previously (Jang et al., 2017). To measure the molecular size and to gain insight into the molecular shape of the protein, we performed the size-exclusion chromatography with multi-angle light scattering experiment. (SEC-MALS). The MALS gives the molecular size of the protein regardless of the molecular shapes. However, the molecular size measured by SEC is deviated from the actual value when the shapes of the proteins is highly elongated. In this study, the molecular weights of VV2_1132 in solution were 135 kDa from MALS and 138 kDa from SEC, both corresponding to a homotetramer (Fig. 1A). The small difference between the measured molecular sizes from different methods further suggest that the tetrameric structure of VV2_1132 is not deviated substantially from the general globular shape. To investigate further the structural features of VV2_1132 and to gain insight into the functions of this protein, the crystal structure of full-length VV2_1132 was determined using Se-anomalous signals from SeMet-substituted crystals. The resulting electron density maps allowed an almost complete model to be built, after which the structure was refined against the 2.2 Å -resolution dataset of the native protein. The asymmetric unit in the crystal contained four molecules tightly interacting with each other, indicating a homotetrameric assembly. This finding is consistent with the SEC-MALS result (Fig. 1). The whole VV2_1132 tetramer adopts the shape of a thick rod and has dimensions of approximately 120 Å × 60 Å × 60 Å (Fig. 1B).

Monomer structure of VV2_1132

Each protomer of VV2_1132 is composed of a DBD (residue 1-100) and an RD (residue 101-304). The overall fold is similar to that of typical LTTRs. The DBD can be divided into three distinct parts: a DNA binding region (1-66), a linker helix (residues 67-90), and a hinge region (residues 91-100) (Fig. 2). The DNA binding region contains a wHTH motif (α2 and α3) that is reinforced by an additional helix (α1). The RD is further divided into two subdomains, RD-I (residues 101-

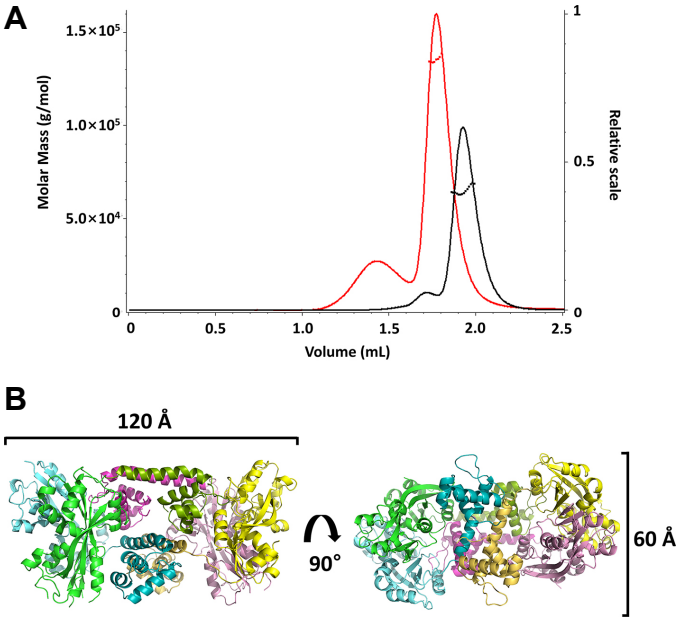

Fig. 1. Oligomeric forms of VV2_1132 in solution and in crystals. (A) SEC-MALS profiles of VV2_1132 (red) and BSA (black). Small squares represent the calculated molar mass (g/mol) in right ordinate axis (135.3 kDa ± 3.3 for VV2_1132, 66.5 kDa for BSA). The relative normalized UV absorbance at 280 nm is drawn with the solid lines in left ordinate axis. Based on the elution volume from the size exclusion chromatography, the molecular size of the VV2_1132 protein is 138 kDa. (B) Structure of the asymmetric unit containing four molecules with two orthogonal views. The four molecules are presented in different colors as follows: Protomer A (dark green and green), protomer B (dark cyan and cyan), protomer C (gold and yellow), and protomer D (magenta and pink).

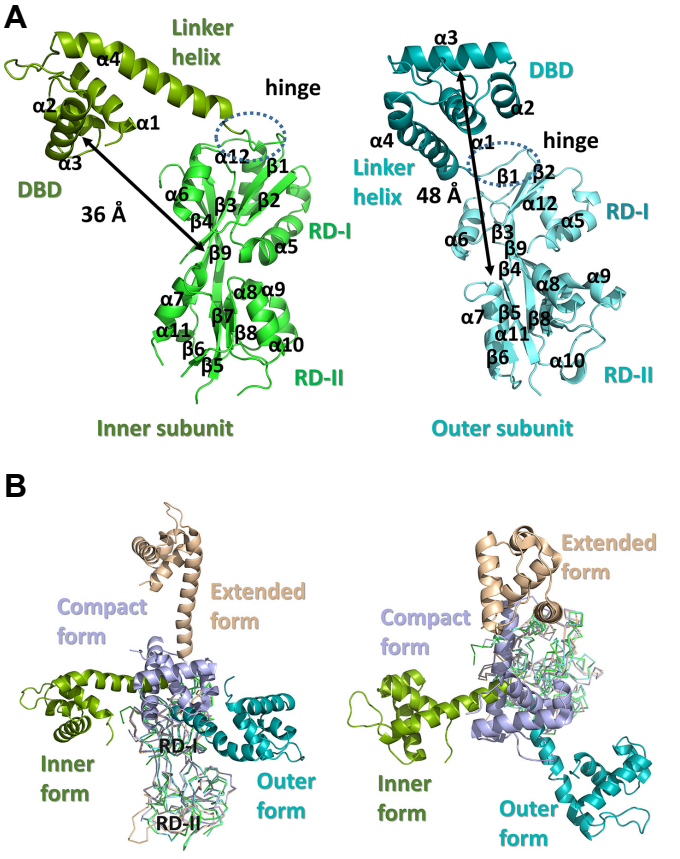

Fig. 2. Protomers in two distinct conformations. (A) Ribbon representations of the subunits in the inner conformation (inner subunits, left) and the outer conformation (outer subunits, right). In the inner subunits, the DBD and RD domains are colored dark green and green, respectively. In the outer subunits, the DBD and RD domains are colored dark cyan and cyan, respectively. The hinge regions are indicated by a circle in a broken line. The distances between the Cα atoms of Phe36, the central residue of the DBD, and Phe206 (the central residue of the RD) are indicated. (B) Structural superposition of four conformations of the LTTR protomers, using the RDs as reference. The panels display a side view (left) and a top view (right). The inner and outer subunits of VV2_1132 are colored dark green and cyan, respectively. The extended and compact subunits of *Pa*OxyR are colored ivory and light blue, respectively. The RDs are in the Cα representations, and the DBDs are in the ribbon representation.

155, 284-300) and RD-II (residues 156-283), both of which adopt a Rossmann-fold topology. The RD-I subdomain is composed of three α helices (α5, α6, and α12) and five β strands (β1, β2, β3, β4, and β9). The RD-II subdomain is composed of five α helices (α7, α8, α9, α10, and α11) and six β strands (β4, β5, β6, β7, β8, and β9) (Fig. 2A).

Typical tetrameric LTTRs such as ArgP, AphB, and OxyR consist of two compact (or closed) subunits and two extended (or open) subunits (Jo et al., 2015; Taylor et al., 2012; Zhou et al., 2010). In the compact subunits, the linker helix of the DBD is in close contact with the RD-I region of the RD, while the DBD is fully spread from the RD in the extended subunit. The VV2_1132 tetramer is composed of two conformationally distinct subunits that are distinguished from both the compact and extended conformations of other LTTRs. We designated the two subunits of VV2_1132 as the inner subunits and the outer subunits (Fig. 2A). The DNA binding motif of the DBD is 36 Å from the center of the RD in the inner subunits, while the DNA binding motif is more than 48 Å from the RD in the outer subunits (Fig. 2A).

We compared the inner and outer subunits of VV2_1132 to the extended and compact subunits of *Pa*OxyR, a representative member of the LTTR family (Jo et al., 2015) (Fig. 2B). Structural superposition using the RDs as references revealed that the linker helices of both VV2_1132 subunits are approximately perpendicular to the axis that runs along RD-I and RD-II, whereas the extended subunit of *Pa*OxyR is roughly continuous with the RD axis. In a top view of the RD, the compact form of *Pa*OxyR is placed in the middle of the inner and outer forms of VV2_1132 (Fig. 2B).

The RD dimer and the DBD dimer

Like in other LTTRs, the VV2_1132 tetramer can be divided into two RD dimers and two DBD dimers because the RDs and DBDs have homophilic interactions, thus forming dimeric units. The overall structures of the VV2_1132 RD dimer and the DBD dimer are similar to those of typical LTTRs. At the interface of the RD dimers, hydrogen bonds between the β2 backbone of RD-I and the β7 backbone of RD-II contribute primarily to the interaction (Fig. 3A). Weak hydrophobic interactions between α6 of RD-I and α9 of RD-II are also partly involved in the dimeric interface (Fig. 3A). In the VV2_1132 DBD dimers, the linker helices in the DBD dimer form the main dimeric interfaces via mostly hydrophobic interactions (Jo et al., 2015) (Fig. 3B).

The interdomain orientation of the RD dimer is affected by the activation state of the LTTR. To determine which state the RD dimer adopts, the VV2_1132 RD dimer was superimposed onto an *E. coli* OxyR RD dimer in the reduced (i.e., inactive) state and the oxidized (i.e., active) state. The superposition showed that the interdomain orientation of the RD dimer is between the two states of the *E. coli* OxyR RD (Fig. 3C). Thus, further study is required to investigate which state this conformation of the RD dimer represents.

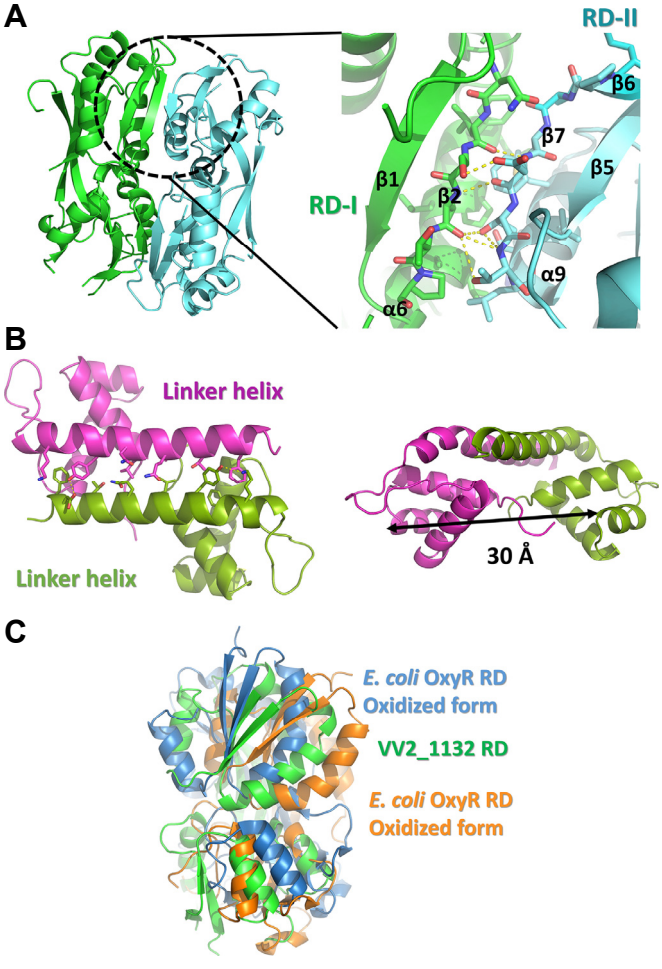

Fig. 3. DBD dimers and RD dimers. (A) RD dimer structure. The major contact site between the RDs in the dimer is indicated by a circle in broken lines (left). The rectangular region is enlarged in the left panel (right). Polar interactions and hydrogen bonds between β2 and β7 are presented in yellow broken lines. (B) Two orthogonal views of the DBD dimer structure. The distance between the two α2 atoms in the DBD dimer is indicated. Residues involved in dimer interaction are presented in stick representation. (C) Structural superposition of the RD dimer of VV2_1132 onto the RD dimer of *E. coli* OxyR (*Ec*OxyR, oxidized form PDB code: 1I6A, reduced form PDB code: 1I69). The oxidized form of *Ec*OxyR is colored bright blue, the reduced form of *Ec*OxyR is orange, and the RD of VV2_1132 is green.

Unique tetrameric structure

In a typical LTTR tetramer, the RD of a compact subunit and the RD of an extended subunit form an RD dimer, as represented by the *Pa*OxyR structure. Likewise, the DBD dimer of typical LTTRs is formed by two subunits adopting different conformations (Fig. 4A). Thus, the tetrameric structure of VV2_1132 is unique out of all other LTTRs whose structures are available. The VV2_1132 DBD dimers are from subunits with the same conformation, unlike the two RD dimers that are from subunits with different conformations. As a result, the 2-fold axes of the tetramers of VV2_1132 and the typical LTTRs are perpendicular to each other, as depicted in Fig. 4A.

The most striking feature is that one of the DBD dimers in the tetramer units is very unlikely to make direct contact with DNA because its DNA binding motifs are hidden within the tetramer, whereas the other DBD dimer has surface-exposed DNA binding motifs. In contrast, both DBD dimers of all other LTTRs can participate in DNA binding. The two DBD dimers of *Pa*OxyR have essentially the same conformation, and the DNA binding motifs of *Pa*OxyR are exposed in the roughly same direction (Fig. 4A, left panel). However, the two DBD dimers of VV2_1132 are stacked vertically along the molecular 2-fold axis and are perpendicular to each other along the 2-fold axis, without any noticeable association between them (Fig. 4A, right panel).

To analyze the VV2_1132 tetramer further, we first focused on the two dimers formed by the RD-RD interface, referred to as RD-type dimers. The two RD-type dimers are equivalent because both are comprised of inner and outer subunits (Fig. 4B). The two DBDs in the RD-type dimer are biased to the inner subunit side, and the DBD of the outer subunit is near the inner subunit RD. No direct contact is made between the outer subunit DBD and the inner subunit RD (Fig. 4B). Unlike RD-type dimers, the two DBD-type dimers (whose dimeric interface is in the DBD) are not equivalent. One of the DBD-type dimers is formed by two inner subunits, while the other DBD-type dimer is formed by two outer subunits. In the DBD-type dimer formed by two inner subunits, the DNA binding motifs are located between the two RDs; thus, the DNA binding motifs are buried in the tetramer (Fig. 4C). In the other DBD-type dimer, the DNA binding motifs are surface-exposed (Fig. 5A). In a DNA docking model based on the BenM DBD structures in complex with DNA (Alanazi et al., 2013), the DNA fragment fit nicely into the DNA binding motif of the DBD dimer consisting of the outer subunits (Fig. 5B).

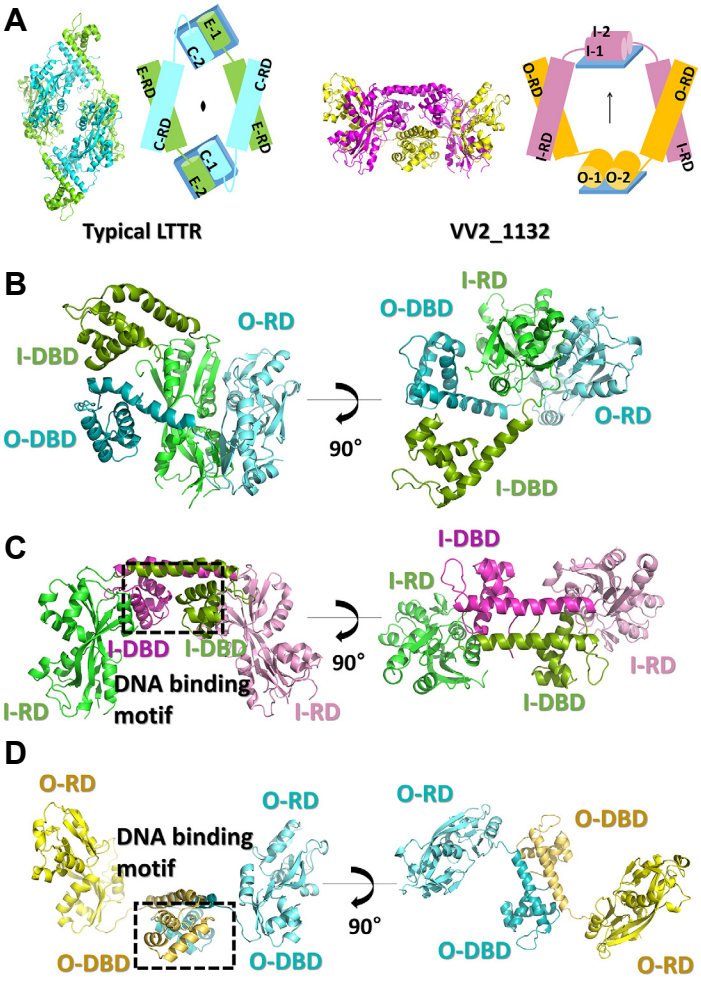

Fig. 4. Tetrameric arrangement of VV2_1132. (A) Comparison of the tetrameric arrangement of a typical LTTR OxyR (left) with that of VV2_1132 (right). The ribbon representation and its corresponding schematic drawing are shown in the same orientation and the same color scheme in each panel. In the schematic drawings, the DBDs are presented in cylinders (for the side views), while the RDs are in rectangles. Extended subunits (E-1 and E-2), compact subunits (C-1 and C-2), inner form subunits (I-1 and I-2), and outer form subunits (O-1 and O-2) are labeled. The blue plates indicate the DNA binding surfaces. The lens symbol in the left panel indicates that the two-fold axis is perpendicular to the plane, and the arrow symbol in the right panel indicates that the two-fold axis is parallel to a vertical line. (B) RD-type dimers of VV2_1132, consisting of an inner subunit and an outer subunit. The two subunits were extracted from the tetramer based on the dimeric interface in the RDs. The DBD and RD in the inner form subunit (I-DBD and I-RD) are colored dark green and green, respectively. The DBD and RD in the outer subunits (O-DBD and O-RD) are colored dark cyan and cyan, respectively. (C) DBD-type dimer consisting of two inner subunits. The inner form subunit is colored dark green or green, whereas the other inner form subunits are colored magenta (I-DBD) or pink (I-RD). The DNA binding motif is denoted by a rectangle. (D) DBD-type dimer consisting of two outer subunits. The second outer subunit is colored dark yellow or yellow (O-DBD or O-RD). The DNA binding motifs are denoted by a rectangle.

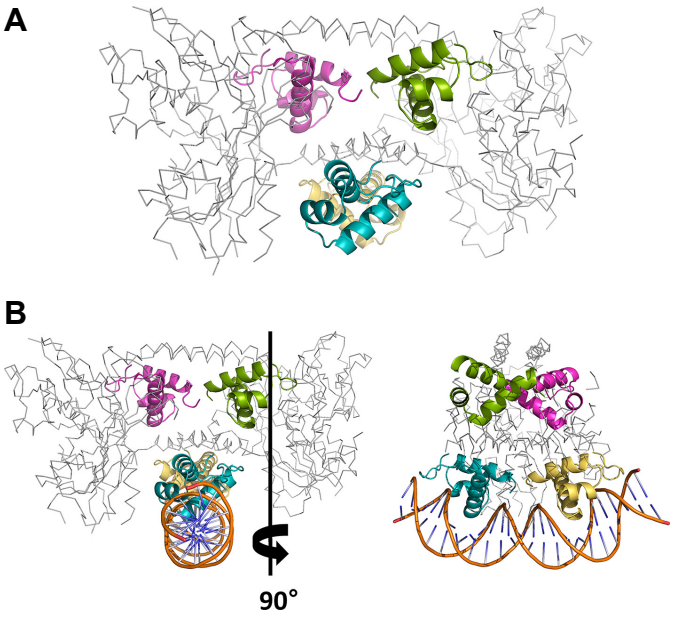

Fig. 5. DNA binding motifs in the tetramer. (A) VV2_1132 tetramer. The DNA binding motifs are highlighted by the ribbon representations. The RDs and linker helices in the DBDs are drawn in the Cα tracing in grey. The DBDs follow the same color scheme as in Fig. 4. (B) VV2_1132 tetramer containing the modeled DNA. The DNA fragment was extracted from the bound DNA to the BenM DBD (PDB code: 4IHT) after superposition onto the VV2_1132 DBD dimers consisting of the outer subunits. Right panel, cross-sectional view along a line.

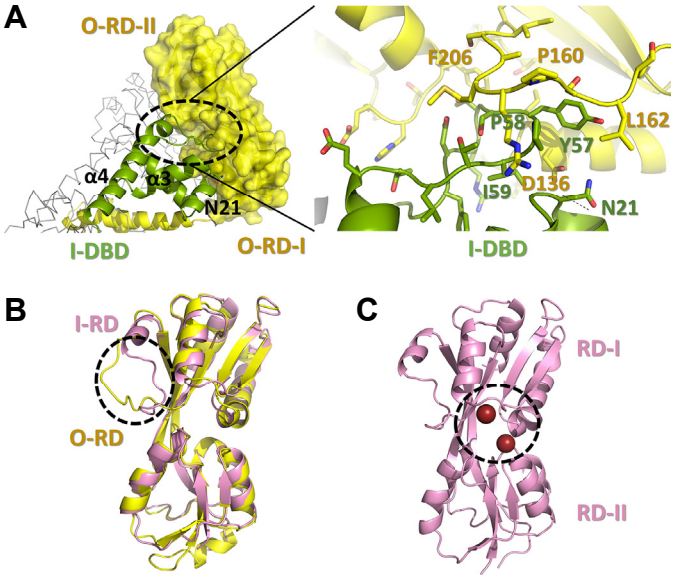

Fig. 6. Putative ligand binding sites. (A) Interaction between the wing loop of protomer A and the putative ligand-binding site of protomer D. The putative ligand-binding site is denoted by a circle and magnified on the right. Residues involved in the interaction are displayed in the right panel. (B) Structure alignment of the protomer C I-RD and the protomer D O-RD. The flexible loop connecting β3 and β4 is highlighted by a circle in a broken line. (C) Bromine ions located in the putative ligand binding site. Bromine ions are presented in red sphere. The putative ligand binding site between the RD-I and RD-II is highlighted by a circle in a broken line.

Putative ligand binding sites

Like most LTTRs, VV2_1132 has small cavities at the ligand binding sites. These cavities are located between the RD-I and RD-II subdomains of the RDs. Since the cavities have been characterized as ligand binding sites in many LTTRs, it is likely that the cavities of VV2_1132 also function as ligand binding sites.

Interestingly, the putative ligand binding sites in the outer subunits are screened mutually by the loops in the DBD of an inner subunit (Fig. 6). A loop connecting α3 and α4 in the DBD of an inner subunit, referred to as a wing in the wHTH domain, blocks entry to the ligand binding site of the RD from the outer subunit via hydrophobic interactions of the Tyr57, Pro58, and Ile59 residues in the DBD and the Pro160, Leu162, and Phe206 residues in the RD (Fig. 6A). Superposition of the inner subunit and the outer subunit of RDs revealed a large movement of the loop of the RD, which interact with the loop of the DBD (Fig. 6B).

We added bromine ions in the crystallization solution as well as the storage buffer. Several bromine ions were found in the putative active sites, indicating that the ligand binding sites have the chemical environment for the bromine ion (Fig. 6C). This observation presents a possibility that the VV2_1132 can bind negatively charged ions or compounds

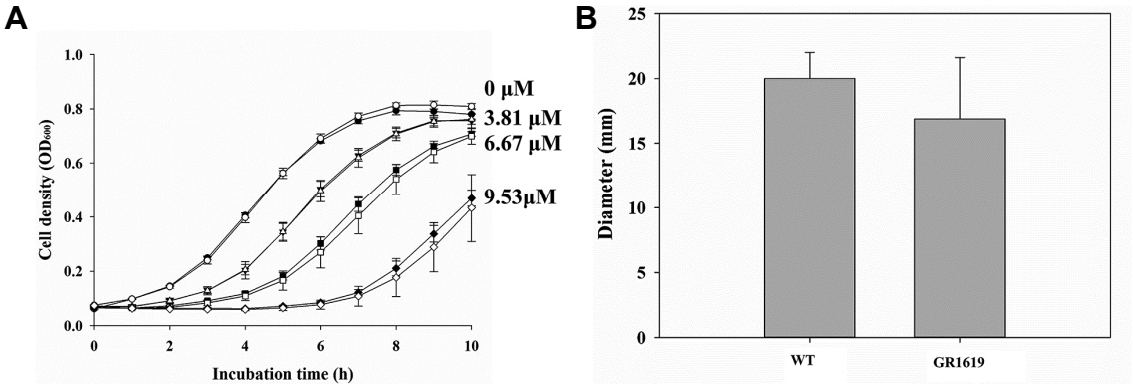

Fig. 7. Phenotypic study of the VV2_1132 gene using wild type *V. vulnificus* and a VV2_1132-deleted *V. vulnificus* strain. (A) Growth kinetics of wild-type *V. vulnificus* (closed symbols) and the VV2_1132 mutant (open symbols) grown in M9 minimal media containing various concentrations of NaOCl were compared as indicated. The growth was monitored spectrophotometrically at 600 nm (OD_{600}). (B) Motility of the *V. vulnificus* strains. The diameters of the motility areas are expressed as means of the results from three independent experiments. Error bars present standard deviation. Statistical significance was determined by *t*-test. No significant difference was observed between the two strains. p=0.355. WT; wild type, GR1619; VV2_1132 mutant.

as ligands. However, the bromine ion is not likely to be specific to the putative active sites because not all the putative ligand binding sites bind the bromine ions.

Functional study of VV2_1132

To explore the function of VV2_1132, we constructed a VV2_1132-deleted *V. vulnificus* CMCP6 strain (GR1619) and compared its resistance to HOCl to that of the wild-type *V. vulnificus* strain. When various concentrations of NaOCl were added to the growth medium, no significant difference was observed between the mutant and wild type strain (Fig. 7A). These results indicate that VV2_1132 is not involved in the HOCl sensitivity of *V. vulnificus*.

Since VV2_1132 is related to *E. coli* QseD, which plays a role in bacterial motility, we next tested the change in cellular motility on semi solid agar after deletion of the VV2_1132 gene. The mutant and wild type strains of *V. vulnificus* were inoculated onto semi solid agar and grown for 18 h. There was no significant difference in motility between the wild type and mutant strains (Fig 7B). Taken together, our results suggest that VV2_1132 might not be related to HOCl sensitivity or motility of *V. vulnificus*. However, we cannot exclude a possibility that VV2_1132 is functionally related to sensing HOCl analogues due to the structural similarity between OCl^- and the bound ion Br^-.

DISCUSSION

Many LTTR structures have been determined. This study presented the crystal structure of VV2_1132 from *V. vulnificus* CMCP6 and showed that VV2_1132 adopts a tetrameric assembly with a novel subunit configuration. In this configuration, only one DBD dimer in the tetramer is involved in DNA binding. Although HypT from *E. coli* and HypT from *S.* Typhimurium showed the highest sequence similarities to VV2_1132, our functional study failed to reveal functional relationship to HOCl sensing or motility regulation. However, it should be noted that the structural properties of bromine ions that were bound to the putative active sites. The binding of bromine ions suggests that VV2_1132 might be functionally related to sensing HOCl analogues or sensing HOCl under special physiological conditions.

It is obvious that the crystal structure does not contain the native ligand and the tetramer of VV2_1132 can bind to a DNA sequence with the DBD dimer in the outer subunits. We observed occlusion of the putative ligand binding sites by the connecting loops in this configuration. This observation suggests that the ligand binding and the DNA binding are coupled. For instance, the ligand binding to the outer subunits may cause a large movement of the DBDs, affecting the transcriptional regulation of this protein.

We next raised the question of how the transcriptional activity of the VV2_1132 tetramer could be regulated by binding of the putative ligand. Since ligand binding would not disrupt the internal tetramer symmetry, the motion induced by ligand binding should be related to the molecular 2-fold rotational axis of the tetramer. Thus, two possible motions can be postulated: 1) spinning of the DBD dimers around the 2-fold axis; and 2) translation of the DBD dimer along the axis. Both of these motions could affect the DNA binding ability of the tetramer. However, ligand-bound structures are required to elucidate the mechanism of regulation. It is of interest to determine the function of the buried DNA binding motifs in the inner subunits in the ligand-bound structures. To connect this novel configuration to the function of the protein, it is necessary to determine the function of the gene, which might be related to the physiology of this highly pathogenic bacterium.

This study provided a complete structure of a new LTTR protein, which showed a novel configuration. This information enriches the structural diversity of the LTTR family. Further studies will focus on revealing the mechanism by which the protein acts as a molecular switch in response to the appropriate ligand.

ACKNOWLEDGMENTS

This research was supported by a grant to NCH and SC from the R&D Convergence Center Support Program, which is funded by the Ministry for Agriculture, Food, and Rural Affairs, Republic of Korea. This work was also supported by a grant from the National Research Foundation of Korea (NRF-2017R1A2B2003992) to NCH. We used the beamline 5C instrument at the Pohang Accelerator Laboratory (Pohang, Republic of Korea). The authors acknowledge the support of Jae-Sung Woo at the Center for RNA Research, Institute for Basic Science (IBS) for assistance in use of SEC/MALS.

REFERENCES

Adams, P.D., Afonine, P.V., Bunkoczi, G., Chen, V.B., Davis, I.W., Echols, N., Headd, J.J., Hung, L.W., Kapral, G.J., Grosse-Kunstleve, R.W., et al. (2010). PHENIX: a comprehensive Python-based system for macromolecular structure solution. Acta Crystallogr. D Biol. Crystallogr. *66*, 213-221.

Alanazi, A.M., Neidle, E.L., and Momany, C. (2013). The DNA-binding domain of BenM reveals the structural basis for the recognition of a T-N11-A sequence motif by LysR-type transcriptional regulators. Acta Crystallogr. D Biol. Crystallogr. *69*, 1995-2007.

Choi, H., Kim, S., Mukhopadhyay, P., Cho, S., Woo, J., Storz, G., and Ryu, S.E. (2001). Structural basis of the redox switch in the OxyR transcription factor. Cell *105*, 103-113.

Drazic, A., Gebendorfer, K.M., Mak, S., Steiner, A., Krause, M., Bepperling, A., and Winter, J. (2014). Tetramers are the activation-competent species of the HOCl-specific transcription factor HypT. J. Biol. Chem. *289*, 977-986.

Drazic, A., Miura, H., Peschek, J., Le, Y., Bach, N.C., Kriehuber, T., and Winter, J. (2013a). Methionine oxidation activates a transcription factor in response to oxidative stress. Proc. Natl. Acad. Sci. USA *110*, 9493-9498.

Drazic, A., Tsoutsoulopoulos, A., Peschek, J., Gundlach, J., Krause, M., Bach, N.C., Gebendorfer, K.M., and Winter, J. (2013b). Role of cysteines in the stability and DNA-binding activity of the hypochlorite-specific transcription factor HypT. PLoS One *8*, e75683.

Emsley, P., and Cowtan, K. (2004). Coot: model-building tools for molecular graphics. Acta Crystallogr. D Biol. Crystallogr. *60*, 2126-2132.

Gebendorfer, K.M., Drazic, A., Le, Y., Gundlach, J., Bepperling, A., Kastenmuller, A., Ganzinger, K.A., Braun, N., Franzmann, T.M., and Winter, J. (2012). Identification of a hypochlorite-specific transcription factor from Escherichia coli. J. Biol. Chem. *287*, 6892-6903.

Guerrero, S.A., Hecht, H.J., Hofmann, B., Biebl, H., and Singh, M. (2001). Production of selenomethionine-labelled proteins using simplified culture conditions and generally applicable host/vector systems. Appl. Microbiol. Biotechnol. *56*, 718-723.

Habdas, B.J., Smart, J., Kaper, J.B., and Sperandio, V. (2010). The LysR-type transcriptional regulator QseD alters type three secretion in enterohemorrhagic Escherichia coli and motility in K-12 Escherichia coli. J. Bacteriol. *192*, 3699-3712.

Jang, K.K., Gil, S.Y., Lim, J.G., and Choi, S.H. (2016). Regulatory characteristics of vibrio vulnificus gbpA gene encoding a mucin-binding protein essential for pathogenesis. J. Biol. Chem. *291*, 5774-5787.

Jang, Y., Choi, G., Jo, I., Choi, S., and Ha, N. (2017). Purification, crystallization, and preliminary X-ray crystallographic analysis of VV2_1132, a LysR-type transcriptional regulator from Vibrio vulnificus. Biodesign *5*, 44-48.

Jo, I., Chung, I.Y., Bae, H.W., Kim, J.S., Song, S., Cho, Y.H., and Ha, N.C. (2015). Structural details of the OxyR peroxide-sensing mechanism. Proc. Natl. Acad. Sci. USA *112*, 6443-6448.

Jo, I., Kim, D., Bang, Y.J., Ahn, J., Choi, S.H., and Ha, N.C. (2017). The hydrogen peroxide hypersensitivity of OxyR2 in Vibrio vulnificus depends on conformational constraints. J. Biol. Chem. *292*, 7223-7232.

Jones, M.K., and Oliver, J.D. (2009). Vibrio vulnificus: disease and pathogenesis. Infect. Immun. *77*, 1723-1733.

Kim, B.S., Hwang, J., Kim, M.H., and Choi, S.H. (2011a). Cooperative regulation of the Vibrio vulnificus nan gene cluster by NanR protein, cAMP receptor protein, and N-acetylmannosamine 6-phosphate. J. Biol. Chem. *286*, 40889-40899.

Kim, H.U., Kim, S.Y., Jeong, H., Kim, T.Y., Kim, J.J., Choy, H.E., Yi, K.Y., Rhee, J.H., and Lee, S.Y. (2011b). Integrative genome-scale metabolic analysis of Vibrio vulnificus for drug targeting and discovery. Mol. Syst. Biol. *7*, 460.

Lim, J.G., and Choi, S.H. (2014). IscR is a global regulator essential for pathogenesis of Vibrio vulnificus and induced by host cells. Infect. Immun. *82*, 569-578.

Lochowska, A., Iwanicka-Nowicka, R., Plochocka, D., and Hryniewicz, M.M. (2001). Functional dissection of the LysR-type CysB transcriptional regulator. Regions important for DNA binding, inducer response, oligomerization, and positive control. J. Biol. Chem. *276*, 2098-2107.

Maddocks, S.E., and Oyston, P.C. (2008). Structure and function of the LysR-type transcriptional regulator (LTTR) family proteins. Microbiology *154*, 3609-3623.

Milton, D.L., O'Toole, R., Horstedt, P., and Wolf-Watz, H. (1996). Flagellin A is essential for the virulence of Vibrio anguillarum. J. Bacteriol. *178*, 1310-1319.

Muraoka, S., Okumura, R., Ogawa, N., Nonaka, T., Miyashita, K., and Senda, T. (2003). Crystal structure of a full-length LysR-type transcriptional regulator, CbnR: unusual combination of two subunit forms and molecular bases for causing and changing DNA bend. J. Mol. Biol. *328*, 555-566.

Otwinowski, Z., and Minor, W. (1997). Processing of X-ray diffraction data collected in oscillation mode. Methods Enzymol. *276*, 307-326.

Park, N., Song, S., Choi, G., Jang, K.K., Jo, I., Choi, S.H., and Ha, N.C. (2017a). Crystal Structure of the Regulatory Domain of AphB from Vibrio vulnificus, a Virulence Gene Regulator. Mol. Cells *40*, 299-306.

Park, S., Ha, S., and Kim, Y. (2017b). The Protein Crystallography Beamlines at the Pohang Light Source II. Biodesign *5*, 30-34.

Sambrook, J., Russell, D.W., and Sambrook, J. (2006). The condensed protocols from Molecular cloning : a laboratory manual (Cold Spring Harbor, N.Y.: Cold Spring Harbor Laboratory Press).

Simon, R., Priefer, U., and Puhler, A. (1983). A broad host range mobilization system for invivo genetic-engineering - transposon mutagenesis in gram-negative bacteria. Bio-Technol *1*, 784-791.

Taylor, J.L., De Silva, R.S., Kovacikova, G., Lin, W., Taylor, R.K., Skorupski, K., and Kull, F.J. (2012). The crystal structure of AphB, a virulence gene activator from Vibrio cholerae, reveals residues that influence its response to oxygen and pH. Mol. Microbiol. *83*, 457-470.

Winn, M.D., Ballard, C.C., Cowtan, K.D., Dodson, E.J., Emsley, P., Evans, P.R., Keegan, R.M., Krissinel, E.B., Leslie, A.G., McCoy, A., et al. (2011). Overview of the CCP4 suite and current developments. Acta Crystallogr. D Biol. Crystallogr. *67*, 235-242.

Zhou, X., Lou, Z., Fu, S., Yang, A., Shen, H., Li, Z., Feng, Y., Bartlam, M., Wang, H., and Rao, Z. (2010). Crystal structure of ArgP from Mycobacterium tuberculosis confirms two distinct conformations of full-length LysR transcriptional regulators and reveals its function in DNA binding and transcriptional regulation. J. Mol. Biol. *396*, 1012-1024.